Implication of the microstructure of binary Cu/ZnO catalysts for their catalytic activity in methanol synthesis

M.M. Günter [a], T. Ressler [a,*], B. Bems [a], C. Büscher [b], T. Genger [b], O. Hinrichsen [b], M. Muhler [b] and R. Schlögl [a]

[a] *Department of Inorganic Chemistry, Fritz-Haber-Institut der Max-Planck-Gesellschaft, Faradayweg 4-6, D-14195 Berlin, Germany*
E-mail: ressler@fhi-berlin.mpg.de

[b] *Lehrstuhl für Technische Chemie, Ruhr-Universität Bochum, D-44870 Bochum, Germany*

Received 28 April 2000; accepted 31 October 2000

Binary Cu/ZnO catalysts with varying molar ratios (90/10 through 10/90) were studied under methanol synthesis conditions at 493 K and at atmospheric pressure. The methanol synthesis activity of the catalysts was correlated to their specific Cu surface area (N_2O reactive frontal chromatography, N_2O RFC) after reduction in 2 vol% H_2 at 513 K. Activity data were supplemented with a detailed analysis of the microstructure, i.e., crystallite size and strain of the reduced Cu and the ZnO phases after reduction using X-ray diffraction line profile analysis. The estimated copper surface area based on a spherical shape of the copper crystallites is in good agreement with data determined by N_2O RFC. A positive correlation of the turnover frequency for methanol production with the observed microstrain of copper in the Cu/ZnO system was found. The results indicate a mutual structural interaction of both components (copper and zinc oxide) in the sense that strained copper particles are stabilized by the unstrained state of the zinc oxide microcrystallites. The observed structural deformation of ZnO in samples with higher Cu loading can originate, for instance, from epitaxial bonding of the oxide lattice to the copper metal, insufficient reduction or residual carbonate due to incomplete thermal decomposition during reduction. Additional EXAFS measurements at the Cu K and the Zn K edge show that about 5% ZnO are dissolved in the CuO matrix of the calcined precursors. Furthermore, it is shown that the microstructural changes (e.g., size and strain) of copper can be traced back to the phase composition of the corresponding hydroxycarbonate precursors.

KEY WORDS: Cu/ZnO catalyst; methanol synthesis; XRD; Voigt profile; Cu surface area; size and strain analysis; TOF; defect structure

1. Introduction

Cu/ZnO catalysts supported on alumina are common catalysts for the hydrogenation of carbon monoxide and carbon dioxide. These systems have found industrial use for low-pressure methanol synthesis and for the low-temperature water–gas shift reaction. It is the proposed synergistic effect in the binary copper/zinc oxide that makes this system interesting for investigations of the effects of structural and chemical promotion [1]. The maximum activity is observed in an intermediate compositional range (~70 mol% Cu), whereas Cu and ZnO alone exhibit only negligible activity [2]. The nature and the location of the active site of this type of catalyst has been the subject of a vast number of publications in both surface science and solid state chemistry. Up to now four major theories concerning the nature of interaction between Cu and ZnO in the system can be found in the literature. Klier [1] proposed copper to be incorporated on interstitial and substitutional sites in the zinc oxide phase assuming three possible valence states Cu^0, Cu^+ and Cu^{2+}. Klier's proposals were made within the framework of bulk defect equilibria based on scanning transmission electron microscopy (STM), X-ray data and optical spectra [3]. Hence, the defect structure and, therefore, the bulk of the catalyst determines the catalytic activity [1]. In a recent publication, Fujitani et al. on the basis of an XRD study corroborated the model of Klier et al. where they interpreted the effect of ZnO on the catalytic activity in terms of a formation of a Cu–Zn surface alloy [4].

In contrast, Waugh et al. suggested that it is merely metallic Cu that carries the catalytic activity and that ZnO is only stabilizing a specific higher Cu surface area [5]. Hence, in their opinion ZnO acts only as an inert support. Waugh's conclusion is based on the observed linear relationship between catalytic activity and copper surface area.

Burch et al. and Spencer claim that ZnO is more than just an inert support [6,7]. Within the sequence of elementary reaction steps in methanol synthesis it is assumed that the hydrogenation of formate adsorbed on metallic copper is enhanced by spillover of hydrogen from ZnO which acts as a reservoir of adsorbed hydrogen.

Topsøe and Topsøe have presented *in situ* IR measurements of 1 and 5% Cu on ZnO catalysts during methanol synthesis [8]. From the observed CO band shift the authors deduced the formation of a surface Cu–Zn alloy upon migration of ZnO moieties onto reduced Cu microcrystallites [6].

In summary, previous investigations of the interaction (*synergy*) of Cu and ZnO have rationalized the real structure of Cu/ZnO catalysts either with morphological changes (dynamic wetting/non-wetting phenomenon) of copper dependent on the oxidation potential [9,10] or as a formation of additional phases (e.g., surface alloy) which leads to an electronic modification [4,11]. The influence of tempera-

* To whom correspondence should be addressed.

1011-372X/01/0100-0037$19.50/0

ture and pH on the preparation of hydroxycarbonate precursors and on the resulting active catalyst has been pointed out by Hadden et al. [12] and Li et al. [13]. An *in situ* structural investigation of the activation of a precursor by combined X-ray absorption and diffraction is reported by Couves et al. [14].

In this study we attempt to reveal correlations between the defective bulk structure and the methanol synthesis activity of Cu/ZnO catalysts. X-ray diffraction line profile analysis is utilized to investigate the bulk structure of copper and zinc oxides with emphasis on those systems that are of industrial interest (∼70 mol% Cu). The employed Voigt deconvolution procedure affords a separation of the origin of the X-ray line broadening into crystallite size and microstrain contributions. In addition, on the basis of X-ray absorption spectroscopy of CuO/ZnO precursors we will show that the phase composition of the multiphasic Cu,Zn-hydroxycarbonate precursor can be related to the microstructure of the resulting Cu phase.

2. Experimental

2.1. Catalyst preparation

Cu/Zn hydroxycarbonate precursors were prepared according to the coprecipitation method at a constant pH of 7.0 from metal nitrate and sodium carbonate solutions. Binary hydroxycarbonate precursors of a systematic series with varying Cu/Zn ratio were obtained (100/0, 90/10, 80/20, 70/30, 60/40, 50/50, 40/60, 30/70, 20/80, 10/90 and 0/100) and are denoted in the following according to their nominal molar ratio. More details about preparation and phases obtained can be found in [15]. 200 mg of each precursor was calcined in a muffle furnace at 600 K for 3 h in static air. Afterwards 20 mg of the obtained mixed oxides were placed in a quartz tube and reduced with 5 vol% H_2 in He (120 ml min^{-1}) applying a heating ramp of 5 K min^{-1} to 523 K and a holding time at 523 K of 2 h. The samples were sealed into 0.3 mm Lindemann capillaries in a glove box (Ar atmosphere with $O_2 \leqslant 1$ ppm, $H_2O \leqslant 1$ ppm) to prevent oxidation of the highly dispersed copper phase.

2.2. Catalytic screening for methanol synthesis activity

The catalytic activity for methanol synthesis was determined using a microreactor set-up which is described in more detail in [16]. The set-up was equipped with a calibrated quadrupole mass spectrometer for quantitative product analysis (Balzers GAM 422). The activity measurements were conducted at 493 K under atmospheric pressure in a glass-lined U-tube reactor using typically 100 mg of 250–355 μm sieve fraction of the catalyst. In the activity measurements the mass balance closed to within 5–10% by the use of He as an internal standard and, hence, the experimental error is estimated to be of similar order of magnitude. Prior to the reaction the sample was reduced in 2 vol% H_2 in He ramping the temperature at 1 K min^{-1} up to 448 K and holding this temperature overnight. Finally, the temperature was increased up to 513 K with a linear heating rate of 1 K min^{-1}. The flow was switched to 100 vol% H_2 until the reduction was completed as verified by mass spectrometry (no further H_2O evolution). The reduction was followed by a Cu area determination performed by passing 1 vol% N_2O in He over the catalyst at 300 K (reactive frontal chromatography [5,17]). For calculation of the exposed Cu surface area a mean surface atom density of 1.47×10^{19} m^{-2} [18] was used. The reproducibility of the surface area determination according to N_2O RFC was ±1%. Methanol synthesis activity was measured at 493 K with a modified space velocity of 500 Nml $(min\ g_{cat})^{-1}$ to determine activities within the kinetically controlled regime.

The composition of the feed gas was 10 vol% CO, 4 vol% CO_2, 72 vol% H_2 in He. The activity of the Cu surface was expressed as a normalized turnover frequency (TOF) defined as the number of product molecules of MeOH formed per surface atom Cu per second, which was normalized to the maximum TOF.

2.3. X-ray absorption spectroscopy and data analysis

XAFS measurements of the calcined precursors (CuO/ZnO samples with Cu/Zn 100/0, 90/10, 80/20 and 0/100) were performed at the Cu K edge ($E = 8.979$ keV) and the Zn K edge ($E = 9.659$ keV) at room temperature in transmission at beamline E4 (HASYLAB, Hamburg). The storage ring operated at 3.6 GeV with injection currents of 150 mA. For the absorption fine structure (EXAFS) analysis, a smooth atomic background, $\mu_0(k)$, was obtained using cubic splines. The radial distribution function FT($\chi(k)$) was obtained by Fourier transforming the k^3-weighted experimental $\chi(k)$ function, multiplied by a Bessel window, into the R space.

2.4. X-ray diffraction and line profile analysis

The XRD experiments were performed on a Stoe transmission diffractometer STADIP-P (Ge primary monochromator, Cu $K_{\alpha 1}$ radiation), equipped with a linear position sensitive detector (PSD, internal resolution 0.01° 2θ). The X-ray diffraction measurements were conducted in the Debye–Scherrer mode with a counting time of 4200 s/step. Copper (Heraeus, purity 99.98%) and zinc oxide (Johnson Mattey, Puratronic, TMI 10 ppm) were used as internal standards for the line profile analysis to correct for instrumental line broadening. A deconvolutive line profile analysis according to the procedure described by Langford et al. could be applied because the symmetric peak profile of the Cu(111) diffraction line [19] was symmetric. The symmetric Voigt function is used to deconvolute a single diffraction peak into the underlying Gaussian and Lorentzian profile contributions. In a first-order approximation the integral breadth of the Gaussian profile is related to strain and disorder in the crystallites, whereas the Lorentzian breadth is

determined by the crystallite size. Further details about this procedure are presented elsewhere [20]. This single peak method is being used because it is particularly suitable in those cases where no higher orders of one crystallographic orientation, as required for a Williamson and Hall analysis [21], are accessible due to obstruction, interference with other peaks or low concentration. In order to estimate a specific copper surface area, $S_{Cu(XRD)}$, based on the XRD crystallite size a spherical shape of the copper crystallite was assumed with the crystallite size as a mean diameter. The surface areas ($S_{Cu(XRD)}$ and $S_{ZnO(XRD)}$) were calculated using a density ρ of 8.92 g cm^{-3} for Cu and 5.673 g cm^{-3} for ZnO [22].

3. Results

3.1. Microstructural characteristics revealed by X-ray diffraction line profile analysis

Figure 1 shows experimental XRD patterns of the series of reduced Cu/ZnO samples. With decreasing copper content (top to bottom) a continuous increase in line width of the Cu 111 and 200 reflection at 43° and 50° 2θ, respectively, is clearly visible. In contrast, the ZnO 100, 002 and 101 lines exhibit a minimum in line width and intensity at a composition of 70/30. No significant narrowing of the ZnO *hkl* lines is observed in the composition range of from 50/50 to 10/90. The results of a detailed Cu 111 and ZnO 100 line profile analysis using a Voigt function are shown in figure 2 (a) and (b), respectively. Both graphs show a conspicuous dependence of Cu and ZnO size and strain on the nominal composition of the samples. For both Cu and ZnO an increase in strain with decreasing crystallite size can be seen. The calculated strain in copper-rich samples (<60 mol% Zn) is small, but a considerable increase in strain can be observed for more diluted samples (60–80 mol% Zn). The crystallite size of Cu shows a continuous decrease from ~1000 Å down to <100 Å from pure Cu to 20 mol% Zn and then remains relatively constant through 80 mol% Zn. For ZnO a monotonous increase in strain with increasing Cu content was obtained. With an increasing Cu concentration, ZnO exhibits a decrease in crystallite size (from 200 Å for pure ZnO down to 120 Å for a sample with 60 mol% Zn). Apparently, the ZnO crystallite growth is retarded by the presence of copper in the samples.

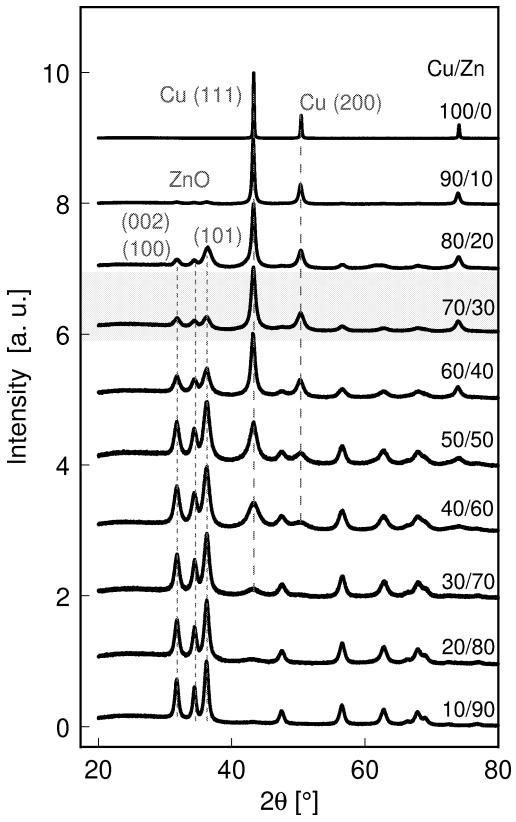

Figure 1. XRD patterns of a systematic series of reduced Cu/ZnO samples. Characteristic *hkl* lines for Cu 111, 200, and ZnO 002, 100, and 101 are indicated. Composition of interest for industrial application is shown in shaded area.

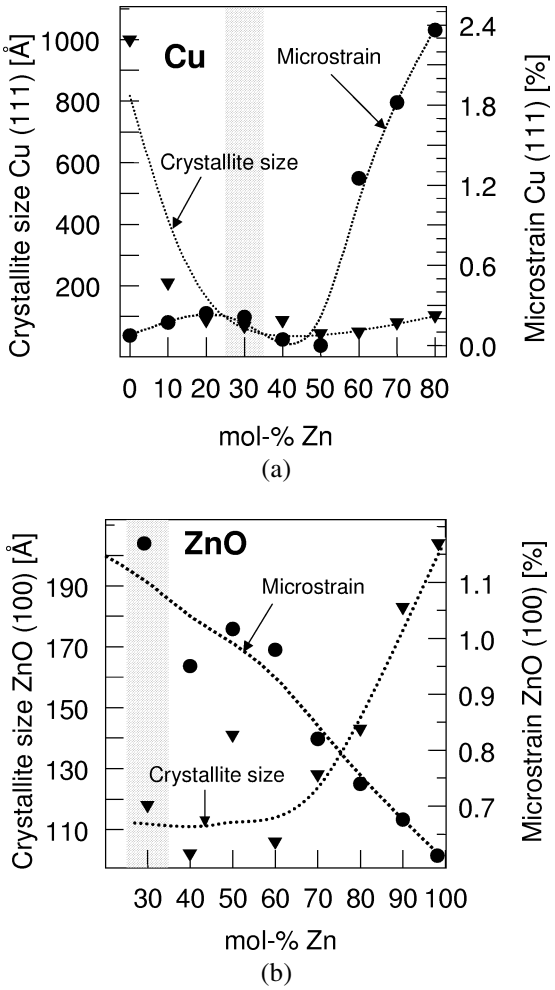

Figure 2. Variation of crystallite size and microstrain of copper (a) and zinc oxide (b) as a function of the nominal composition after reduction at 523 K in 5 vol% H_2 in He. The data are based on the analysis of the copper(111) peak and the ZnO(100) peak. Composition of interest for industrial application is shown in the shaded area.

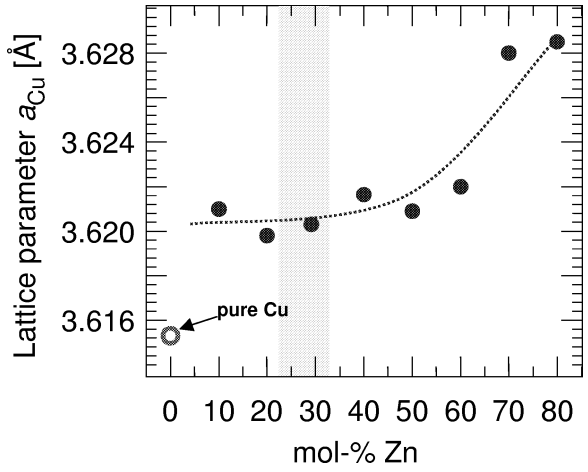

Figure 3. Variation of the Cu lattice parameter a with Zn content after reduction in 2 vol% H_2 at 523 K (measured at RT). Composition of interest for industrial application is shown in shaded area.

In figure 3 the refined Cu lattice constant a (fcc, Fm3m, $a = 3.6150$ Å [23]) is depicted with increasing Zn content. Already at a Zn concentration of 10 mol% a considerable lattice expansion ($\Delta a_{Cu}/a_{0,Cu} \approx 0.14\%$) can be observed. In the range from 90/10 to 40/60 the Cu lattice constant does not change significantly, whereas at Zn concentrations of 70 and 80% mol% a strong lattice expansion is obtained ($\Delta a_{Cu}/a_{0,Cu} \approx 0.35\%$).

Experimental transformed EXAFS $\chi(k)$ of pure ZnO, CuO obtained from decomposition of malachite and calcined binary samples with 10 and 20 mol% Zn are depicted in figure 4. A significant difference in the imaginary part of the FT($\chi(k)$) for the sample 10/90 at about 2.5 Å (indicated with an arrow) is observed compared to that of ZnO (figure 4(a)). This deviation is less pronounced for the imaginary part of the FT($\chi(k)$) of sample 80/20 which resembles more that of ZnO. The Cu K edge FT($\chi(k)$) spectra of the samples 90/10 and 80/20 exhibit a considerable reduction in amplitude at above 3 Å compared to the FT($\chi(k)$) of CuO (lower part of figure 4).

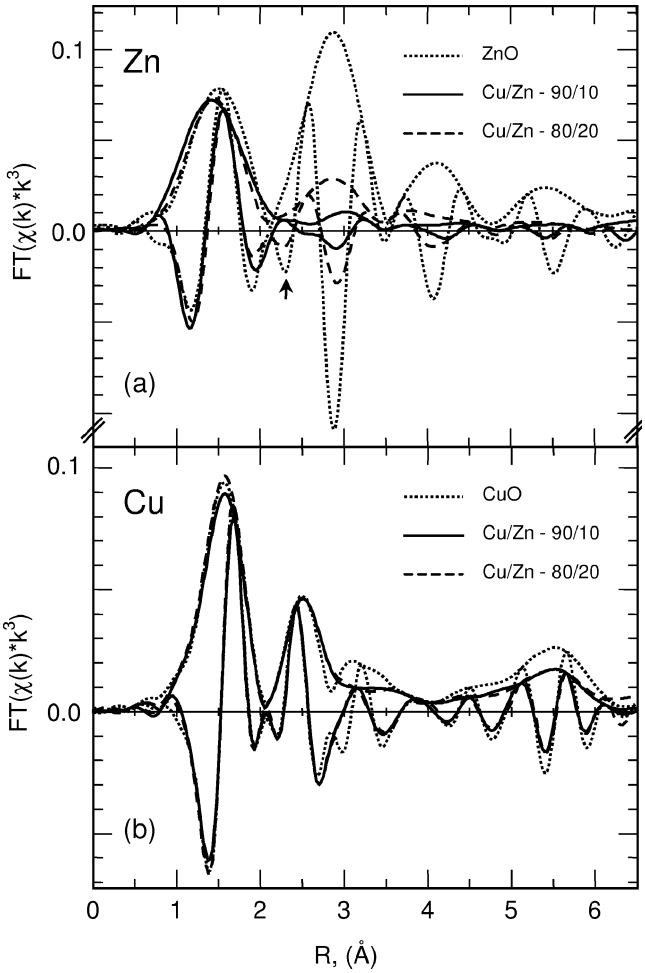

Figure 4. Experimental Fourier transformed Zn K edge $\chi(k)$ (magnitude and imaginary part) of ZnO, and calcined samples with Cu/Zn of 90/10 and 80/20 (a); and experimental FT($\chi(k)$) of Cu K edge of CuO and calcined samples with Cu/Zn of 90/10 and 80/20 (b).

3.2. Copper surface area measurements

Figure 5 shows the dependence of the specific copper surface area, determined by N_2O RFC ($S_{Cu(N_2O)}$) or estimated using the crystallite size determined by XRD ($S_{Cu(XRD)}$), on Zn concentration. It can be seen that the "XRD surface areas" $S_{Cu(XRD)}$ on the average are higher than the $S_{Cu(N_2O)}$ values. This difference may originate from a small degree of agglomeration of copper particles or support interactions which reduce the accessible Cu surface area. In addition, a varying Cu particle size distribution could result in differences in surface areas. The deviation of $S_{Cu(XRD)}$ from $S_{Cu(N_2O)}$ appears to be more pronounced in the intermediate composition range. However, in total, both surface areas are in good agreement, which underlines the applicability of the XRD surface area calculation. Hence, the reliable copper surface area based on

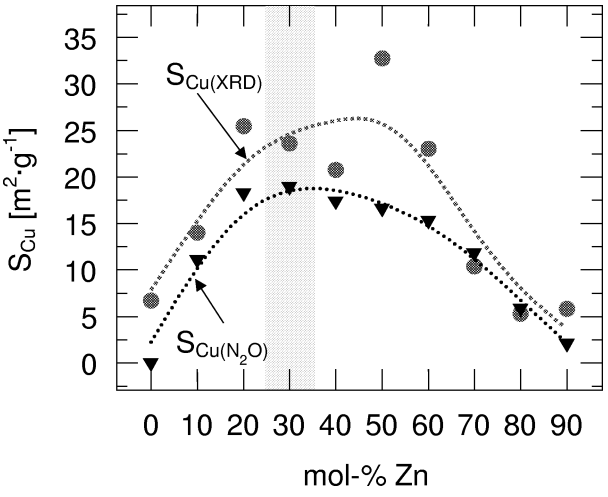

Figure 5. Copper surface area as a function of the nominal composition. Values are determined either by N_2O RFC ($S_{Cu(N_2O)}$) or estimated using the crystallite size determined by XRD ($S_{Cu(XRD)}$). Composition of interest for industrial application is shown in the shaded area.

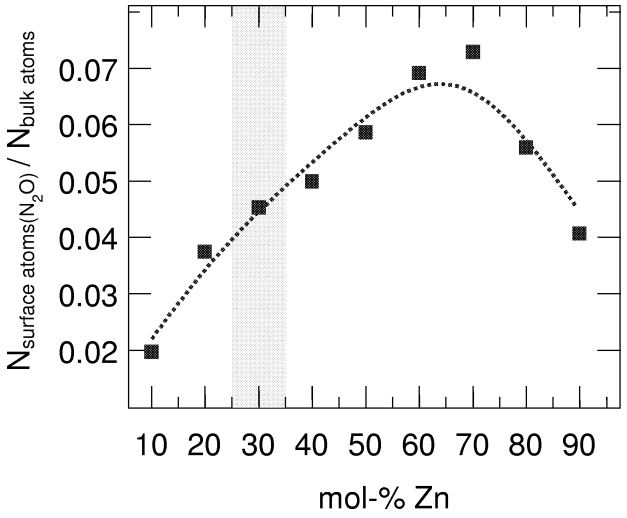

Figure 6. Ratio of copper surface atoms determined by N_2O RFC to bulk atoms from XRD crystallite size assuming a spherical shape as a function of the Zn content. Composition of interest for industrial application is shown in the shaded area.

N_2O RFC and the nominal Cu content of the sample permits to calculate the ratio of copper surface atoms to those in the bulk in order to obtain an estimation of the Cu dispersion. Figure 6 shows an increase of dispersion of copper atoms in terms of $N_{\text{surface atoms}(N_2O)}/N_{\text{bulk atoms}}$ with increasing Zn concentration reaching a maximum at a composition of 70 mol% Zn.

3.3. Catalytic activity screening

In agreement with previous investigations [5] the methanol synthesis activity of the Cu/ZnO samples studied proved to be strongly dependent on the nominal composition. The methanol production rate as a function of composition shows a volcano type behavior, as depicted in figure 7. The maximum in normalized production rate is obtained for the sample with a composition of Cu/Zn = 80/20, in good agreement with previous publications [2]. An approximately linear dependence of the normalized methanol production rate on the Cu surface area is obtained Joyner et al. [24]. This would imply a constant TOF independent of the composition with no other structural parameters influencing the catalytic activity. In order to clarify if, in addition to the Cu surface area, other structural parameters affect the methanol synthesis activity of the samples studied, the normalized turnover frequency as a function of the Zn content is shown in figure 9. Evidently, deviations from the supposedly constant TOF with increasing Zn content exist. A minimum in normalized TOF is observed for those samples that exhibit basically no microstructural strain according to figure 2(a). For higher Zn concentration (>70 mol% Zn) a considerable increase in TOF can be seen, indicating that other parameters in addition to the Cu surface area determine the methanol synthesis activity.

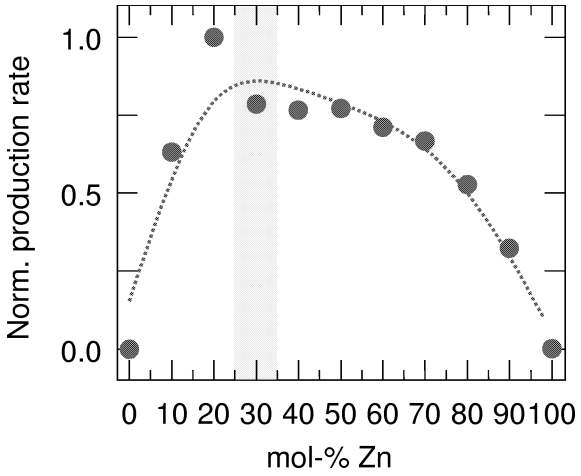

Figure 7. Normalized production rate of methanol with increasing Zn concentration. The reaction was carried out at 493 K under atmospheric pressure with a feed gas composition of 10% CO, 4% CO_2, 72% H_2 in He.

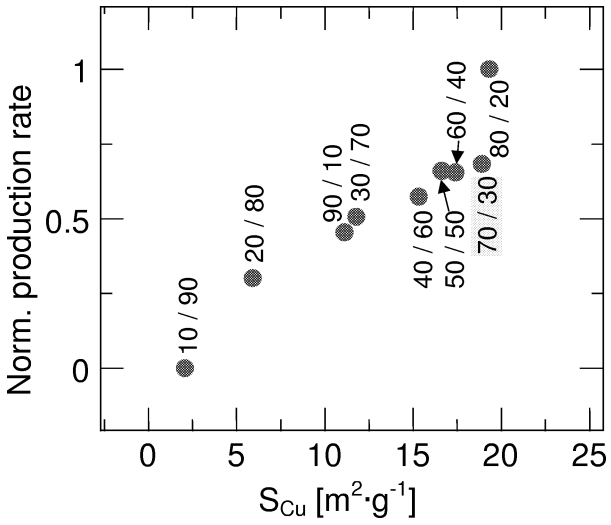

Figure 8. Normalized methanol production rate as a function of copper metal surface area. Composition of interest for industrial application is shown in the shaded area.

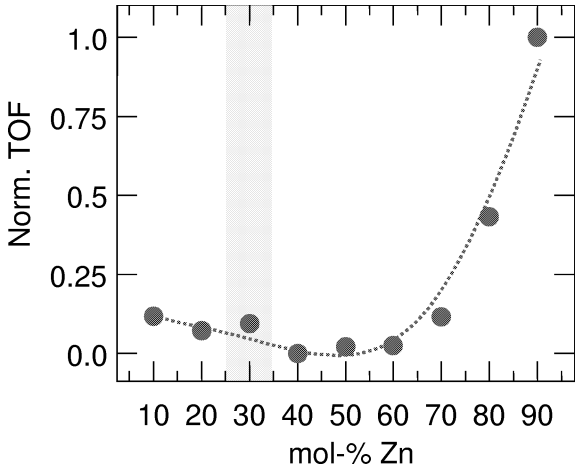

Figure 9. Normalized turnover frequency (TOF) for methanol production as a function of Zn content. Composition of interest for industrial application is shown in the shaded area.

4. Discussion

4.1. Impact of the Cu microstructure on the methanol synthesis activity

The normalized TOF for methanol production as a function of the copper lattice strain is displayed in figure 10. Evidently, the TOF for methanol production on the Cu/ZnO systems studied exhibits a positive correlation with the microstrain in the Cu crystallites. Hence, a higher turnover frequency is attained for strained copper particles. It appears that a high Cu surface area is a necessary prerequisite for an active Cu/ZnO catalyst but that other microstructural parameters also affect methanol synthesis activity.

Correlation of the TOF for methanol production with the degree of dispersion estimated from the $S_{Cu(N_2O)}$ surface area (figure 6) is depicted in figure 11(a). It can be seen that the TOF cannot unequivocally be correlated to the degree of dispersion. Interestingly, two groups of samples can be observed. One group (A in figure 11(a)) shows a constant TOF independent of the degree of dispersion, whereas the other group (B in figure 11(a)) exhibits a decreasing TOF with increasing dispersion. The behavior of the group B samples can be ascribed to the increased contribution of the Cu strain in these systems which is enhanced by a slight increase in crystallite size for more diluted samples (e.g., sample 10/90). While maintaining a similar crystallite size as that of the 30 mol% Zn the more diluted and strained samples expose a more active surface for methanol synthesis. In contrast, the group A samples exhibit no significant strain contributions. Furthermore, it can be seen that Cu/ZnO samples that are of interest for industrial applications (<60 mol% Zn) do not possess the most highly dispersed crystallites as it has been claimed in the literature with respect to, e.g., the dynamic spreading behavior of Cu on ZnO [9].

The correlation of TOF and Cu lattice strain presented in this work indicates that a combination of Cu surface area and Cu and ZnO microstructural strain determines the methanol synthesis activity of Cu/ZnO catalysts. Our results substantiate the assumption of Topsøe and Topsøe [11] that strain would be one possible explanation for the strong CO band shift which was previously observed with FTIR by Kampshoff et al. [25]. The origin of the microstrain observed can be explained by (i) a certain fraction of the minority phase dissolved in the bulk of the majority phase (e.g., ZnO in Cu), or (ii) incomplete reduction and hence residual oxygen in the Cu matrix, (iii) interfacial strain caused by epitaxial bonding of Cu on ZnO. Increased CO adsorption energies on strained surfaces have been predicted on the basis of self-consistent density functional calculations in [26]. The model described therein could, in principle, be extended to the adsorption properties of hydrogen on metal surfaces.

In figure 11(b) the normalized TOF for methanol production is shown as a function of the Cu lattice parameter a. Only the sample 20/80 shows a significant increase in the TOF with expansion of the Cu lattice. In a previous publication Fujitani and Nakamura [27] have assigned the observed increase in Cu lattice parameter to a Cu–Zn alloy formation

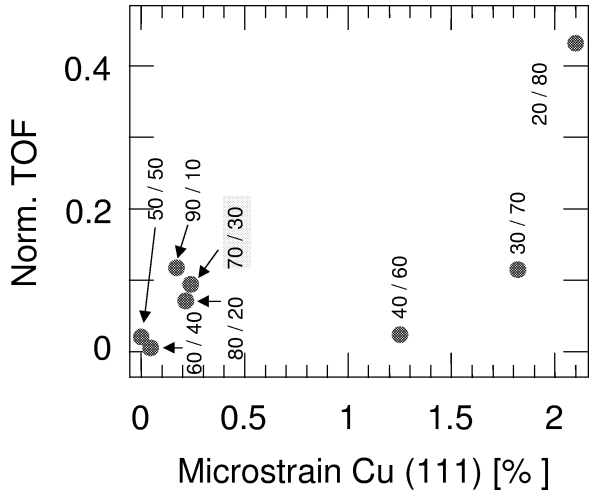

Figure 10. Normalized turnover frequency (TOF) for methanol production as a function of the Cu microstrain derived for the Cu(111) peak.

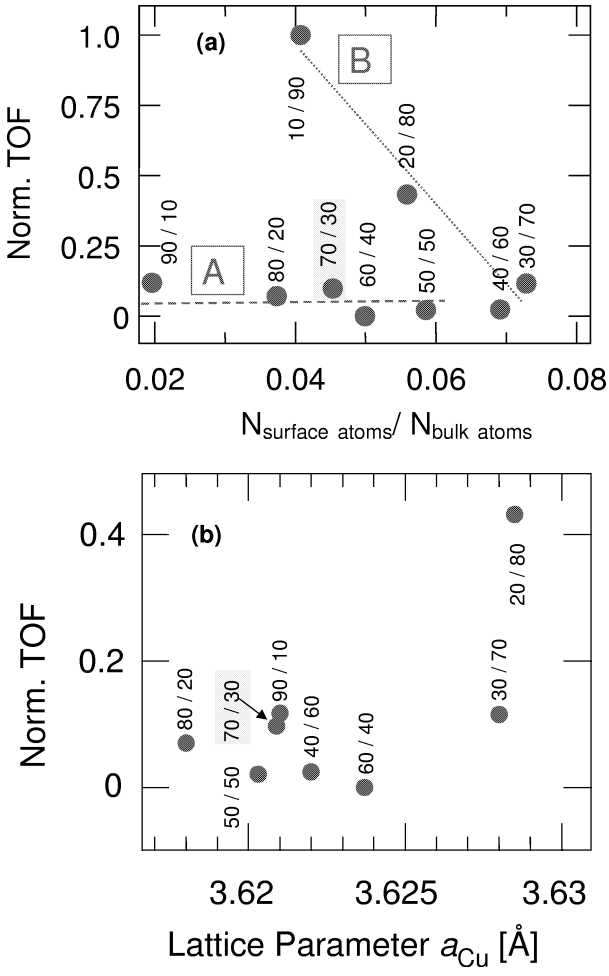

Figure 11. Normalized turnover frequency (TOF) for methanol production as a function of (a) the copper atom dispersion (expressed as the ratio of Cu surface atoms determined by N_2O RFC to the number of the bulk atoms based on XRD crystallite size determination), (b) the copper lattice parameter a.

and, hence, have identified this alloy phase as being responsible for an increasing methanol production activity. Compared to the Cu lattice parameter of monophasic α-brass [28] the lattice expansion obtained corresponds to 5 mol% Zn dissolved in Cu. The amount of Zn dissolved in Cu appears to be constant up to 60 mol% Zn. Evidently, the assumption of ZnO incorporated in the CuO bulk is corroborated by the EXAFS measurements (figure 4). The change in short-range order of ZnO and CuO in samples with 10 mol% Zn cannot be ascribed to a crystallite size effect because XRD measurements on the oxide precursors yielded an average crystallite size for CuO of ∼75 Å. EXAFS data analysis using theoretical phases and amplitudes of CuO yielded an enlarged metal–metal distance for shells above 3 Å. This indicates that Zn may occupy specific Cu sites in the CuO lattice rather than being randomly distributed. It has been shown in the literature that CuO can form solid solutions with several bivalent cations (e.g., Mg, Co, Zn and Ni, concentration <10 mol%) [29]. Therefore, we propose that the inclusion or solid solutions of ZnO in the CuO bulk enables the formation of a Cu–Zn alloy at a temperature of 523 K. Otherwise, temperatures above 900 K would be required for the formation of brass from ZnO and CuO under reducing conditions. The dissolution of Zn in CuO may cause both the Cu lattice expansion and the Cu microstrain measured in the reduced Cu/ZnO catalysts.

Binary Cu/ZnO samples of industrial interest possess Cu crystallites in the range of 100–200 Å. Obviously, XRD is a suitable method to investigate microstructural parameters (e.g., size and strain) within this crystallite size regime. Other techniques that are more surface sensitive or probe the short-range structural order (e.g., IR and EXAFS) require smaller cluster sizes to elucidate the minor structural changes in the systems described in this work. Therefore, mostly copper loadings that are less relevant for industrial application have been investigated and it needs to be kept in mind that results obtained for smaller copper clusters may not be directly transferable to the catalysts used in industry.

4.2. Effect of precursor phases on Cu and ZnO microstructure

A phase assignment of the hydroxycarbonate phases obtained from a coprecipitation procedure at constant pH based on XRD and thermoanalytical data is described in detail elsewhere [15]. Three multiphasic composition ranges in the hydroxycarbonate precursors can be distinguished as a function of composition. The first region extends from 0 to ∼15 mol% Zn and encompasses the pure malachite phase ($Cu_2(OH)_2CO_3$) as well as the zincian-malachite phase ($(Cu,Zn)_2(OH)_2CO_3$). The second region extends from 20 to ∼50 mol% Zn and encompasses the transition from the zincian malachite to the aurichalcite phase ($(Cu,Zn)_5(OH)_6(CO_3)_2$). The third region at a Zn concentration larger than 50 mol% encompasses the transition of aurichalcite to the hydrozincite phase ($Zn(OH)_6(CO_3)_2$). A possible dissolution of ZnO in CuO as evidenced by the EXAFS results may be related to the crystal structure of zincian malachite (rosasite) in which Zn and Cu cations occupy non-equivalent sites [30]. After mild calcination the local arrangement is preserved which could result in the observed Zn "ordering" in the CuO matrix. Taking into account the discontinuous behavior of the Cu/ZnO microstructure (e.g., lattice parameter and microstrain, figures 3 and 2(a), respectively) and the pronounced particle growth of ZnO (figure 2(b)) above a certain composition threshold (>60 mol% Zn) it is reasonable to assume that the precursor phase composition directly influences the resulting Cu microstructure and in turn the performance (e.g., TOF) of the resulting Cu/ZnO catalyst. Therefore, on the basis of the results presented here, we conclude that the Cu-containing hydrozincite phase, upon calcination and reduction, preferentially affords microstrained Cu crystallites which exhibit a higher intrinsic methanol synthesis activity (see figure 8). There is only a seemingly discrepancy between our findings and other experimental work by Spencer concerning the precursor phase affording a maximum activity [7]. In his publication the activity is given as an absolute production rate expressed per weight catalyst, whereas we refer to an intrinsic rate in terms of TOF for the most active catalyst. Nevertheless, a maximum in absolute production rate is attained for a sample with ∼30 mol% Zn stemming from an zincian-malachite precursor which is similar to the results by Spencer. Therefore, we propose that an optimum catalyst should feature both a high Cu surface area and strained Cu clusters.

5. Summary

A complete series of binary Cu/ZnO samples was subjected to methanol synthesis screening experiments. It was found that the production rate of methanol is not a linear function of the specific Cu surface area over the entire Cu/ZnO composition range. XRD line profile analysis revealed a considerable microstructural strain in both Cu and ZnO in some samples. Furthermore, it was shown that the TOF of methanol synthesis is directly correlated to the strain in the Cu metal phase. This experimental evidence clearly indicates that the specific Cu surface area of Cu/ZnO samples alone cannot unequivocally account for the observed methanol production rates of these systems. Structural defects of Cu resulting from ZnO in Cu, incomplete reduction or epitaxial orientation to ZnO are believed to cause strain which modifies the Cu surface area and, thus, influences the catalytic activity.

Furthermore, changes in the microstructure of both copper and ZnO (i.e., size, strain, and lattice parameter) were found to coincide with changes in phase composition of the hydroxycarbonate precursors (structure of zincian malachite and the transition from the aurichalcite-rich to a Cu containing hydrozincite phase composition). The formation of ZnO–CuO solid solutions (∼5% ZnO in CuO) was detected which may lead after reduction to the formation of Cu–Zn al-

loy. For a compositional range of more than 60 mol% Zn the strained Cu crystallites expose a Cu surface which is more active than that of a 30 mol% Zn catalyst. Hence, it is concluded that the phase composition of the hydroxycarbonate precursor directly influences the active phase of the Cu/ZnO catalyst.

Acknowledgement

The authors want to acknowledge Rolf Jentoft, Daniel Herein and Josef Find for valuable discussions. One of the authors (TR) thanks the Deutsche Forschungsgemeinschaft "DFG" for financial support (Habilitationstipendium).

References

[1] K. Klier, Adv. Catal. 31 (1982) 243.
[2] B.S. Rasmussen, P.E.H. Nielsen, J. Villadsen and J.B. Hansen, in: *Preparation of Catalysts IV*, eds. B. Delmon, P. Grange, P.A. Jacobs and G. Poncelet (Elsevier, Amsterdam, 1987) p. 785.
[3] K. Klier, Appl. Surf. Sci. 19 (1984) 267.
[4] J. Nakamura, I. Nakamura, T. Uchijima, T. Wantanabe and T. Fujitani, Stud. Surf. Sci. Catal. 101 (1996) 1389.
[5] G.C. Chinchen and K.C. Waugh, Appl. Catal. 25 (1986) 101.
[6] R. Burch, S.E. Golunski and M.S. Spencer, J. Chem. Soc. Faraday Trans. 86 (1990) 2683.
[7] M.S. Spencer, Topics Catal. 8 (1999) 259.
[8] N.-Y. Topsøe and H. Topsøe, Topics Catal. 8 (1999) 267.
[9] C.V. Ovesen, B.S. Clausen, J. Schiøtz, P. Stoltze, H. Topsøe and J.K. Nørskov, J. Catal. 168 (1997) 133.
[10] B.S. Clausen, J. Schiøtz, L. Gråbæk, C.V. Ovesen, K.W. Jacobsen, J.K. Nørskov and H. Topsøe, Topics Catal. 1 (1994) 367.
[11] N.-Y. Topsøe and H. Topsøe, J. Mol. Catal. A 141 (1999) 95.
[12] R.A. Hadden, P.J. Lambert and C. Ranson, Appl. Catal. 122 (1995) L1.
[13] J.-L. Li and T. Inui, Appl. Catal. A 137 (1996) 105.
[14] J.W. Couves, J.M. Thomas, D. Waller, R.H. Jones, A.J. Dent, G.E. Derbshire and G.N. Greaves, Nature 354 (1991) 465.
[15] B. Bems, M.M. Günter, D. Herein, M. Schur and R. Schlögl, in preparation.
[16] O. Hinrichsen, T. Genger and M. Muhler, Chem.-Ing.-Tech. 72 (2000) 94.
[17] G.C. Chinchen, C.M. Hay, H.D. Vanderwell and K.C. Waugh, J. Catal. 103 (1987) 79.
[18] J.R. Anderson and K.C. Pratt, *Introduction to Characterization and Testing of Catalysts* (Academic Press, New York, 1985).
[19] J.I. Langford, J. Appl. Crystallogr. 11 (1978) 10.
[20] M.M. Günter, T. Ressler, B. Bems and R. Schlögl, in preparation.
[21] G.K. Williamson and W.H. Hall, Acta Metall. Mater. 1 (1953) 22.
[22] D.R. Lide and H.P.R. Frederikse, eds., *The CRC Handbook of Chemistry and Physics: a Ready-Reference Book of Chemical and Physical Data*, 80th Ed. (CRC, Boca Raton, FL, 1999).
[23] H.E. Swanson and E. Tatge, Natl. Bur. Stand. (US) Circ. 539, I (1953) 15.
[24] R.W. Joyner, Catal. Lett. 6 (1990) 151;
R. Burch, S.E. Golunski and M.S. Spencer, Catal. Lett. 6 (1990) 155, and references therein.
[25] E. Kampshoff, E. Hahn and K. Kern, Phys. Rev. Lett. 73 (1994) 704.
[26] M. Mavrikis, B. Hammer and J.K. Nørskov, Phys. Rev. Lett. 81 (1998) 2819.
[27] T. Fujitani and J. Nakamura, Catal. Lett. 56 (1998) 119.
[28] S.S. Rao and T.R. Anantharaman, Curr. Sci. 32 (1963) 262.
[29] C. Delorme, Bull. Soc. Franc. Mineral. 81 (1958) 19.
[30] A.C. Roberts, Powder Diffraction 1 (1986) 1.